Journal Pre-proofs

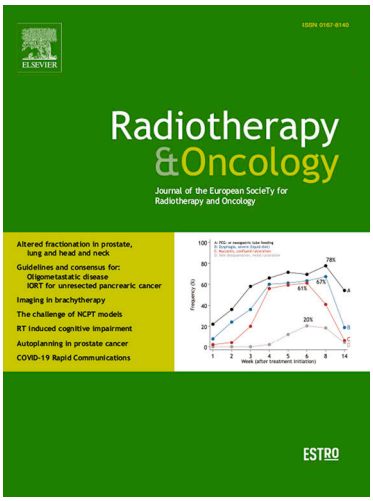

Original Article

Relationships between rectal and perirectal doses and rectal bleeding or tenesmus in pooled voxel-based analysis of 3 randomised phase III trials

M. Marcello, J.W. Denham, A. Kennedy, A. Haworth, A. Steigler, P.B. Greer, L.C. Holloway, J.A. Dowling, M.G. Jameson, D. Roach, D.J. Joseph, S.L. Gulliford, D.P. Dearnaley, M.R. Sydes, E. Hall, M.A. Ebert

PII: S0167-8140(20)30696-4
DOI: https://doi.org/10.1016/j.radonc.2020.07.048
Reference: RADION 8463

To appear in: *Radiotherapy and Oncology*

Received Date: 13 February 2020
Revised Date: 25 July 2020
Accepted Date: 28 July 2020

Please cite this article as: Marcello, M., Denham, J.W., Kennedy, A., Haworth, A., Steigler, A., Greer, P.B., Holloway, L.C., Dowling, J.A., Jameson, M.G., Roach, D., Joseph, D.J., Gulliford, S.L., Dearnaley, D.P., Sydes, M.R., Hall, E., Ebert, M.A., Relationships between rectal and perirectal doses and rectal bleeding or tenesmus in pooled voxel-based analysis of 3 randomised phase III trials, *Radiotherapy and Oncology* (2020), doi: https://doi.org/10.1016/j.radonc.2020.07.048

Relationships between rectal and perirectal doses and rectal bleeding or tenesmus in pooled voxel-based analysis of 3 randomised phase III trials

Keywords: External beam radiotherapy (EBRT), prostate cancer, gastrointestinal toxicity, rectal bleeding, tenesmus, voxel-based analysis, dose-toxicity relationships

M Marcello MSc, BSc [a, b]
JW Denham MD, FRANZCR [c]
A Kennedy BSc(Hons) [b]
A Haworth FACPSEM, PhD, MSc, BSc(Hons) [d]
A Steigler BMath [e]
PB Greer PhD, MSc, BSc [f, g]
LC Holloway PhD, BSc [h, i, j]
JA Dowling PhD, BComp(Hons I), BAppSc [f, k]
MG Jameson PhD, B.Med.Rad.PhysSc(Hons) [h, i, j, l]
D Roach MSc, BS [h, i, l]
DJ Joseph MD, FRANZCR, MRACMA [m, n, o]
SL Gulliford PhD, MSc(Hons), BSc(Hons) [p, q]
DP Dearnaley MA, MD, FRCR, FRCP [r]
MR Sydes MSc, CStat [s]
E Hall PhD, CStat [t]
MA Ebert PhD, BSc(Hons) [a, b, n]

[a] Department of Physics, University of Western Australia, Western Australia, Australia
(Address: 35 Stirling Highway, Crawley, WA, 6009, Australia)

[b] Department of Radiation Oncology, Sir Charles Gairdner Hospital, Western Australia, Australia
(Address: Hospital Avenue, Nedlands, WA, 6009, Australia)

[c] School of Medicine and Public Health, University of Newcastle, New South Wales, Australia
(Address: University Drive, Callaghan, NSW, 2308, Australia)

[d] School of Physics, University of Sydney, New South Wales, Australia
(Address: Physics Road, Camperdown, NSW, 2006, Australia)

[e] Prostate Cancer Trials Group, School of Medicine and Public Health, University of Newcastle, New South Wales, Australia
(Address: University Drive, Callaghan, NSW, 2308, Australia)

[f] School of Mathematical and Physical Sciences, University of Newcastle, New South Wales, Australia
(Address: University Drive, Callaghan, NSW, 2308, Australia)

[g] Department of Radiation Oncology, Calvary Mater Newcastle, New South Wales, Australia
(Address: Corner of Edith & Platt Street, Waratah, NSW, 2298, Australia)

[h] Department of Medical Physics, Liverpool Cancer Centre, New South Wales, Australia
(Address: 1 Campbell Street, Liverpool, NSW, 2170, Australia)

[i] South Western Sydney Clinical School, University of New South Wales, New South Wales, Australia
(Address: Goulburn Street, Liverpool, NSW, 2170, Australia)

[j] Centre for Medical Radiation Physics, University of Wollongong, New South Wales, Australia
(Address: Northfields Avenue, Wollongong, NSW, 2522, Australia)

[k] CSIRO, Queensland, Australia
(Address: Butterfield Street, Herston QLD 4029, Australia)

[l] Cancer Research Team, Ingham Institute for Applied Medical Research, New South Wales, Australia
(Address: 1 Campbell Street, Liverpool, NSW, 2170, Australia)

[m] School of Surgery, University of Western Australia, Western Australia, Australia
(Address: 35 Stirling Highway, Crawley, WA, 6009, Australia)

[n] 5D Clinics, Claremont, Western Australia, Australia
(Address: 261 Stirling Highway, Claremont, WA, 6010, Australia)

[o] GenesisCare WA, Western Australia, Australia
(Address: 24 Salvado Road, Wembley, WA, 6014, Australia)

[p] Radiotherapy Department, University College London Hospitals NHS Foundation Trust, London, United Kingdom
(Address: Gower Street, Bloomsbury, London, WC1E 6BT, United Kingdom)

[q] Department of Medical Physics and Biomedical Engineering, University College London, London, UK
(Address: Gower Street, Bloomsbury, London, WC1E 6BT, United Kingdom)

[r] Academic UroOncology Unit, The Institute of Cancer Research and the Royal Marsden NHS Trust, London, United Kingdom
(Address: 15 Cotswold Road, Sutton, London, SM2 5NG, Australia)

[s] MRC Clinical Trials Unit, Institute of Clinical Trials and Methodology, University College London, United Kingdom
(Address: 90 High Holborn, London, WC1B 9LJ, United Kingdom)

[t] Clinical Trials and Statistics Unit, The Institute of Cancer Research, London, United Kingdom
(Address: 15 Cotswold Rd, Sutton, SM2 5NG, United Kingdom)

Corresponding author details:
Mr Marco Marcello
Department of Physics
University of Western Australia
Tel: 0439 940 621
Email: 20739859@student.uwa.edu.au

DATA SHARING STATEMENT

The data from this study was derived from three clinical trials (the RADAR, RT01 and CHHiP trials). The authors do not own these data and hence are not permitted to share them in the original form (only in aggregate form, e.g., publications).

ABSTRACT

Background and purpose: This study aimed to identify anatomically-localised regions where planned radiotherapy dose is associated with gastrointestinal toxicities in healthy tissues throughout the pelvic anatomy.

Materials and methods: Planned dose distributions for up to 657 patients of the Trans Tasman Radiation Oncology Group 03.04 RADAR trial were deformably registered onto a single exemplar computed tomography dataset. Voxel-based multiple comparison permutation dose difference testing, Cox regression modelling and LASSO feature selection were used to identify regions where dose-increase was associated with grade≥2 rectal bleeding (RB) or tenesmus, according to the LENT/SOMA scale. This was externally validated by registering dose distributions from the RT01 (n=388) and CHHiP (n=241) trials onto the same exemplar and repeating the tests on each of these data sets, and on all three datasets combined.

Results: Voxel-based Cox regression and permutation dose difference testing revealed regions where increased dose was correlated with gastrointestinal toxicity. Grade≥2 RB was associated with posteriorly extended lateral beams that manifested high doses (> 55 Gy) in a small rectal volume adjacent to the clinical target volume. A correlation was found between grade≥2 tenesmus and increased low-intermediate dose (~25 Gy) at the posterior beam region, including the posterior rectum and perirectal fat space (PRFS).

Conclusions: The serial response of the rectum with respect to RB has been demonstrated in patients with posteriorly extended lateral beams. Similarly, the parallel response of the PRFS with respect to tenesmus has been demonstrated in patients treated with the posterior beam.

INTRODUCTION

Gastrointestinal (GI) symptoms remain a commonly-reported side-effect of prostate external beam radiotherapy (EBRT)[1,2], despite improvements in precision from new technologies such as image guided intensity modulated radiotherapy (IG-IMRT)[3]. Improving the accuracy of predictive toxicity models, through further understanding of the relationship between anatomically localised dose and toxicity, will help optimise organ at risk (OAR) dose constraints. Most current models provide constraints based on information from dose-volume histograms (DVHs) describing planned dose to whole OARs[4,5,6,7]. This ignores heterogeneous intra-organ radio-sensitivity, which can be investigated through spatial dose information in the three-dimensional (3D) planned distribution not utilised by whole-organ DVHs. Voxel-based analyses, in which anatomically localised dose-toxicity relationships are identified on the surface or within the volume of OARs, can determine radiosensitive symptom related subregions (SRSs) of OARs from which more optimal dose constraints may be derived.

Several studies have begun to investigate rectal dose-sensitivity in this manner. Munbodh et al were the first study to comprehensively explore the relationship between rectal surface areas irradiated and the spatial distribution of the dose in the development of late rectal toxicity, revealing that increased irradiated rectal surface area was associated with toxicity[8]. Buettner et al also investigated the relationship between late rectal toxicities and spatial features from rectal dose-surface maps[9]. Rectal bleeding (RB) and loose stools were shown to be more strongly correlated with these features than rectal dose-surface histograms (DSH). This group proceeded to parameterise the 3D dose distribution to the rectum and correlate resulting features with late RB, loose stools, and a global toxicity score[10]. These features predicted all three endpoints more accurately than standard DVHs. In a similar analysis by Moulton et al, spatial features of rectal dose-surface maps related to dose shape and coverage were shown to correlate strongly with a range of late GI complications[11]. More recently, Onjukka et al[12]

and Heemsbergen et al[13] have continued to demonstrate localised rectal surface dose-toxicity correlations. Other voxel-based studies have identified predictive rectal subregions[14,15]. DVHs derived from these subregions (found within the inferior-anterior rectum) were demonstrated to be more predictive than whole-rectum DVHs.

No study to date, however, has performed a voxel-based analysis searching for correlation between variation in planned dose within individual voxels and GI toxicity throughout the entire pelvic anatomy. This analysis is the first to operate without the assumption that dose-toxicity correlations necessarily occur at OARs, as both OAR and non-OAR voxels are part of the pelvic space included in the analysis. This has provided an opportunity to confirm or undermine previously observed dose-toxicity relationships, including previous predictive SRSs. It may also illuminate dose-response pathology that defies assumptions of responsible anatomy. Furthermore, this is the first study enabling the exploration of how broader pelvic dose patterns relate to toxicity, revealing the impact of factors related to treatment technique, such as beam arrangement.

In this study, multiple voxel-based statistical methods were employed to investigate the association between 3D planned dose and measures of GI toxicity in the entire pelvic anatomy. Many shortcomings have typically hindered recent voxel-based analyses[16,17], including misregistration of planned 3D dose distributions, false positive rates due to the large number of voxels being statistically compared, not using time-to-event data, or not controlling for patient baseline characteristics. This study used a combination of statistical approaches to compensate these shortcomings. High quality planned dose data from three prospective multi-centre prostate radiotherapy clinical trials was utilised in order to assess the consistency of derived associations across cohorts, participating centres, employed radiotherapy techniques and overall treatment approach. 'External validation' was defined as applying the same voxel-based tests to datasets from two other trials, with one trial providing a cohort similar to that of the primary dataset and the other substantially different (primarily in terms of treatment technique). This validation aimed to determine whether the emergent dose-toxicity patterns within the primary dataset were generalisable to these (similar and different) external datasets. This validation also had an exploratory element, in that it enabled the identification of new emergent patterns in the external datasets regardless of whether they matched the patterns in the primary datasets.

METHODS AND MATERIALS

Clinical Trials

Table 1 describes the three clinical trials from which data was sourced for this study. 3D planned dose distributions, with corresponding computed tomography (CT) images including delineated clinical target volume (CTV), rectum and bladder collected by the RADAR trial, were utilised as the primary dataset of this study. Similar information was collected in the RT01 and CHHiP trials and utilised as external validation datasets.

3D Data Preparation

Three CT image registration templates were chosen from an independent cohort of 39 prostate EBRT patients[18]. Pairwise registrations of CT images within this cohort along with registrations between this cohort and the RADAR CT dataset were used to generate a normalised cross correlation similarity matrix. This matrix was used to perform clustering by affinity propagation to select the single most representative patient CT as an exemplar from the initial cohort. This exemplar was the first registration template (T1). Next, an anti-exemplar, most-different from T1, was chosen as a template on which the impact of registration and reference geometry could be tested (T2). Finally, a similar process was used to select a cropped exemplar, enabling analysis to be restricted to a small region

including the prostate and immediate surrounding organs (T3). Dose distributions were then deformed onto these templates through application of deformation vector fields obtained from the image-based registrations above. See Appendix Section 2 for images of templates (with voxel sizes) and registration pipelines. The 3D dose distributions from all phases of radiotherapy were summed together according to biologically isoeffective 2 Gy per fraction dose (EQD2)[19], using a spatially invariant alpha/beta ratio of 3, resulting in a single distribution for each patient registered onto each template. All subsequent analyses used dose distributions which uniformly sampled 1 in 2 voxels from each spatial dimension for T1 and T2 (due to the large number of total voxels). That is, every second voxel in the x direction, every second voxel in the y direction, and every second voxel in the z direction were included, resulting in the sampling of one eighth of the original total number of voxels. For T3, every voxel was used.

Gastrointestinal Toxicity Outcomes

Two time-to-event GI toxicity outcome measures were included for analysis: rectal bleeding and tenesmus. An event consisted of the first peak grade≥2 occurrence during follow-up. All patients who reported baseline symptoms of grade≥1 were removed from analysis, apart from RT01 tenesmus patients as this information was not available. Physician assisted toxicity grading was performed according to the Late Effects on Normal Tissue, Subjective, Objective, Management, Analytic (LENT/SOMA) questionnaire[20]. For RADAR, patients were routinely followed up, post-treatment, every 3 months to 18 months, every 6 months to 5 years, and then annually. RT01 patients were assessed at 6, 12, 18, and 24 months after commencing radiotherapy, and annually thereafter. CHHiP patients were assessed for late toxicities beginning 26 weeks after the start of radiotherapy and every 6 months for 2 years, and then yearly.

Voxel-Based Dose Difference Permutation Test

It is recommended that Figure 1 is closely followed while reading through the following descriptions of the voxel-based tests. This test was performed according to the process outlined by Chen et al[16], utilising their multiple comparisons permutation method. Following Figure 1, for each given outcome patients were divided according to whether they experienced an event at any time during follow-up. The mean dose distributions of each group were then compared to each other, voxel-by-voxel, to reveal regions of statistically significant dose difference. This method utilises a nonparametric permutation-based test in which the group labels are randomly swapped (permuted) and the dose-comparison repeated for each permutation. In this study, 1000 permutations were performed generating a distribution of test statistics. A threshold was derived from this distribution, used to determine the region of dose difference with statistical certainty. This method accounts for the multiple statistical testing problem arising from comparing a vast number of voxels (see Appendix A of Chen et al for more detail). The dose difference region is produced by thresholding at any chosen p-value. That is, voxels with a mean dose difference between patients with and without an outcome event at any desired p-value can be determined. In this study, thresholds of $p<0.05$, $p<0.1$, $p<0.2$ and $p<0.3$ were applied to thoroughly explore the dose difference. As shown in Figure 1, the mean dose difference map was imposed on the registration template, including the delineated CTV, bladder and rectum. If the dose difference reached statistical significance at one of the given p-value thresholds, then the voxels corresponding to this difference (the thresholded p-value map) were highlighted in green and imposed onto the dose difference map.

Uni-Voxel Cox Regression Test

This test generated a separate Cox proportional hazards model for each voxel (hence, ‘uni’-voxel), testing the dose-toxicity association in that voxel. Taking a given voxel, patients were divided into

two groups about the median of the distribution of dose values across the cohort, as in Figure 1. The hazard ratio (HR) of toxicity between the high dose group and low dose group was then calculated, with a corresponding p-value testing whether HR>1 or HR<1 at the statistical level using a two-tailed z-test from the MATLAB coxphfit function. This HR therefore compares the incidence of toxicity between each dose group, indicating the dose-toxicity relationship at the given voxel. Age, prescribed dose, disease risk, cancer stage, baseline prostate specific antigen (PSA) concentration and number of treatment beams were patient factors investigated as potential control variables in each model, attempting to eliminate their confounding influence at each voxel[21,22]. These controls were chosen through an automated selection process (see Appendix Section 1 for details). Repeating this process for every voxel produced a 3D HR map and corresponding p-value map revealing the dose-toxicity across the pelvic anatomy. The continuous HR map was first imposed on the anatomical template. Following this, the thresholded p-value map was imposed onto the HR map, showing (in green) voxels where HR < 1 or HR > 1 at the $p < 0.05$ level.

Multi-Voxel Cox Regression Test with LASSO Feature Selection

In contrast to the uni-voxel Cox regression test, this test combined all voxel-dose variables in the pelvic anatomy into a single multivariate Cox regression model (hence, 'multi'-voxel). The LASSO (Least Absolute Shrinkage Selection Operator[23]) was then applied (using the glmnet package on MATLAB) to select voxels with dose-variables that did not correlate with each other in the model, while still correlating strongly with the outcome. The LASSO requires a pre-specified variable, λ, that determines the threshold by which features or variables (voxels) in the Cox model are selected. As λ increases, more features are excluded, until none are selected. 100 values of λ were pre-specified, equally spaced from that which selected all voxels to that which selected none. For each value of λ, one-in-ten cross validation was used to test the predictive ability of the resulting Cox model – the model comprised of the voxels selected by the LASSO. The final value of λ was that which maximised the corresponding model's ability to predict the outcome by minimising the partial likelihood deviance. The selected voxels were then imposed on the anatomical template, indicating whether HR > 1 or HR < 1 in each case. As with the uni-voxel Cox regression test, HRs in this test compared the incidence of the outcome (e.g. tenesmus) between the high dose group and low dose group at a given voxel, with the cut-point for dose determined in the same way. The LASSO enabled selection of voxels strongly correlated with the outcome while accounting for inter-voxel dose correlation and the multiple testing problem.

Analysis Details

Firstly, all three voxel-based tests were performed on all three registration templates for the RADAR dataset only. This was an internal validation to determine whether emergent dose-toxicity patterns on T1 would also appear on T2 and T3, thus ascertaining whether the choice of registration template impacted these patterns. The results for this component of the analysis are found in Section 3 of the Appendix. Next, an external validation was performed by repeating the tests on the T1 template only for the RT01, CHHiP and Combined datasets (as the previous component conducted on T2 and T3 were sufficient for the purpose of determining the impact of registration). The combined dataset represented an attempt to maximise outcome event rates and anatomical dose variation, increasing statistical power, and observe the emergent patterns.

All components of the above analysis were undertaken for both the RB and tenesmus toxicity outcomes. The voxel-based dose difference permutation and uni-voxel Cox regression tests were performed using MATLAB R2016b and later versions (MathWorks, Natick MA), while the multi-voxel LASSO test was performed on R 3.6.1 (The R Foundation, Vienna). All 3D results were displayed using ITK-SNAP version 3.8.0[24].

RESULTS

Table 2 shows the number of patients from each trial included in the analyses, with corresponding patient baseline characteristic and outcome information, after patients were excluded due to loss of follow-up, missing data, and considering only patients receiving EBRT alone. For RADAR, 6 and 11 early (≤3 months) toxicity events were included for RB and tenesmus respectively. All other toxicity events for all other datasets were late (>3 months).

The three voxel-based tests identified voxel clusters (VCs) and individual voxels across the pelvic anatomy where dose variation was associated with both GI toxicity outcome measures. The following paragraph presents the major finding from the internal validation that tested the impact of the choice of registration template on the results. The next paragraph presents the results for RB across all datasets, mostly following Figure 2. The dominant dose-RB association pattern across all tests and datasets was identified by locating correlative VCs and individual voxels on slices from results maps. Less consistent patterns were similarly identified. The final paragraph presents the results identified for tenesmus in the same way, following Figure 3.

The dose-toxicity patterns from the RADAR datasets on T1 were generally reproduced on the other registration templates (T2 and T3). The patterns were distorted according to the anatomical difference between the templates, but otherwise were similar, suggesting the revealed dose-toxicity association patterns are largely independent of choice of registration template (see Appendix Section 3 for these results).

Figure 2 shows the results for RB. The dominant pattern is an association between increased RB and posteriorly extended lateral beam margins culminating in higher dose at the rectum adjacent to the CTV centre. Dose difference maps from all trial cohorts and the combined cohort ("Combined") exhibit this pattern. In particular, the axial planes show RB patients having between approximately 4 and 7 Gy more dose on average than non-RB patients where lateral beams extend posteriorly into the rectal space. The corresponding sagittal planes reveal RB patients have between 4 and 5 Gy more dose on average in a sub-volume of the rectum adjacent to the CTV, statistically different at $p<0.3$ for Combined. Figure 4 shows the mean and standard deviation (SD) dose distributions for the Combined cohort. A representative voxel was selected in the identified sub-volume adjacent to the CTV to compare doses of patients with and without rectal bleeding here. Figure 4 reveals that Combined patients with and without rectal bleeding had an average dose of 57.3 Gy and 53.0 Gy in this voxel respectively (SD=14.2 Gy). The corresponding uni-voxel HR maps confirm these patterns for all datasets, revealing VCs with HR>1 in the same regions, with $p<0.05$ for all cohorts but CHHiP. For CHHiP, VCs with HR>1 ($p<0.05$) were found directly posterior to the rectum. For Combined, the multi-voxel LASSO selected voxels in regions corresponding to where the uni-voxel test revealed associations, with one HR>1 voxel selected at the rectum adjacent to the CTV, visible in the sagittal plane. Increased RB is associated with reduced dose in the anterior beam region for Combined, with HR<1 ($p<0.05$) VCs found here by both the permutation and uni-voxel tests. Less prominently, a correlation is present between increased RB and increased dose in the posterior oblique beam regions for RT01, revealed in the corresponding uni-voxel HR map.

The results for tenesmus are displayed in Figure 3. The most consistent pattern is an association between increased tenesmus and increased dose at the posterior rectum extending posteriorly where the posterior beam is expected to contribute dose. This is clearly seen in the RADAR, CHHiP and Combined results. The permutation test identified VCs of significant dose difference in this posterior region, where patients with tenesmus have up to 4 Gy more dose for RADAR ($p<0.3$) and Combined ($p<0.05$), with this region being larger and less fragmented for Combined. Figure 4a) shows that

Combined patients with and without tenesmus had an average dose of 24.2 Gy and 21.1 Gy at a voxel in this VC directly posterior to the rectum. The same figure shows the dose-effect region is broad – extending across approximately two thirds of the rectum in the superior-inferior direction and to the surface from the rectum posterior. The uni-voxel HR maps reveal VCs with HR>1 ($p<0.05$) in this same region for RADAR, CHHiP and Combined. For RT01, the same correlation pattern is present, but is weaker, with HR>1 ($p>0.05$) VCs present in this posterior region. The multi-voxel LASSO confirmed this association for Combined by selecting several voxels with HR>1 in the space postero-inferior to the rectum, most visible in the coronal plane. Reduced dose in the anterior beam region near the surface is associated with increased tenesmus for Combined, where patients with tenesmus have up to 3.5 Gy less dose ($p<0.05$), confirmed by the corresponding uni-voxel HR map. Reduced dose is also associated with tenesmus in the oblique and lateral beam regions for Combined, and in the posterior obliques only for RADAR.

DISCUSSION

In this study, quality-assured and reviewed planning data collected in multi-centre clinical trials with extensive follow-up was used to derive independent datasets for analysis. Subsequent associations between voxel-dose and measures of GI toxicity across the pelvic anatomy have been identified without assuming associations necessarily occur at organ sites. Although no individual voxel-based test in this study addressed every typical shortcoming of voxel-based analyses, each test did address particular shortcomings such that a consistent result across all techniques could be considered independent of these issues.

Rectal bleeding was consistently correlated with increased dose in rectal sub-volumes adjacent to the CTV centre, manifesting in patients treated with posteriorly extended lateral beams. This sub-volume is located at the boundary of the high-dose region. Moving directly posteriorly from the CTV, this sub-volume coincides almost exactly with the maximum standard deviation in dose in the combined cohort along this plane. Therefore, this association is most likely not indicating that this rectal sub-volume is particularly radiosensitive relative to the rest of the rectum. It is more likely that a dose-bleeding effect is highlighted within this particular sub-volume because it is located in both the high-dose region and in a region of sufficient dose variation to reveal this statistical effect.

All three trials allowed 70 Gy to 15% of the rectal volume. Patients with posteriorly extended lateral beams may have plans that met dose-volume constraints while still resulting in high doses (up to 70 Gy) to small volumes (up to 15%) of the rectum, resulting in RB. This comports with studies that have established correlations between high doses to small volumes of the rectum and RB across multiple treatment modalities[25,6,26,27,28,29]. 98.1% of grade≥2 RB events in the combined cohort were late (>3 months). Late radiation damage includes progressive obliterative endarteritis that leads to ischaemia and fibrosis of the rectal tissue, ulcerating and eroding rectal blood vessels, resulting in bleeding[30]. This study provides the first 3D evidence of the serial response of the rectum with respect to late rectal bleeding without the assumption that dose-toxicity effects necessarily occur at organ sites, while relating this effect to treatment technique. It is therefore recommended that posterior extension of lateral beams be done with an awareness of the potential to produce rectal hotspots associated with RB.

In contrast to RB, tenesmus was correlated with increased dose in the posterior beam region and decreased dose in the posterior oblique beam regions. Correlation coincided with the posterior perirectal fat space (PRFS). The dose-effect here was distributed across a broad volume and was in the low-intermediate dose-range (~25Gy). Therefore, the effect may be due to increased low-intermediate doses broadly distributed in the PRFS. Ebert et al have shown a dose-tenesmus response at the anal canal and anorectum in the low-intermediate dose range (5-38 Gy)[25]. Moulton et al have

similarly demonstrated an association between tenesmus and greater low-intermediate doses (20-30 Gy) to the inferior 20% and lateral-posterior of the rectum in combined EBRT and high dose-rate brachytherapy patients[11]. An association between increased low-intermediate doses (10-40 Gy) throughout the PRFS and grade≥2 tenesmus was demonstrated by Gulliford et al, suggesting the PRFS responds as a parallel structure with respect to control related toxicities[31]. Similarly to the Moulton et al and Ebert et al studies mentioned above, Onjukka et al demonstrated an association between faecal incontinence (another control related symptom) and increased irradiation of the caudal anal canal[12]. These findings are broadly consistent with this study, noting that the first three of these studies utilised patients from the RADAR trial. The PRFS facilitates rectal motility, compliance and control, and contains a large number of sympathetic, parasympathetic and non-autonomic nerve fibres[31]. Damage to this region may therefore lead to nerve dysfunction, contributing to control related symptoms such as tenesmus. The broad posterior beam association found here confirms the PRFS behaving as a parallel structure with respect to tenesmus. The posterior beam should be used with an awareness of this behaviour. Landoni et al observed that mean rectal dose was associated with faecal incontinence (another control related symptom)[6], while Cicchetti et al demonstrated that mid-range doses to large volumes of the rectum were associated with stool frequency and rectal pain (also control related symptoms). Both these findings suggest a parallel response of the rectum itself with respect to control related symptoms. Similarly, in this study, it cannot be ruled out that dose in the posterior beam is a surrogate for dose to the entire rectum and therefore the rectum itself may be exhibiting parallel behaviour with respect to tenesmus rather than or along with the PRFS.

3D-CRT dose distributions typically result in more dose to surrounding OARs than modern techniques such as IG-IMRT. Sourcing 3D-CRT dose distributions therefore helped power the study due to this increased signal (i.e., dose) at OARs and resulting increased toxicity outcome rates (for RADAR and RT01 datasets). For low-medium income countries that still predominantly use 3D-CRT, the results presented here are relevant. However, for higher income countries that use more conformal modern techniques, the results may not be as applicable. In particular, the rectal dose hotspot correlated with RB may require rectal doses that are uncommon in these treatments. The tenesmus correlation, in the low-intermediate dose-range, may still be relevant.

The relationships presented here are correlations that may or may not represent anatomically-localised physiological-caused dose-toxicity associations. Only the uni-voxel Cox regression accounted for patient related factors, and these represent only a sample of possible factors that could confound the identified dose-toxicity relationships. To ensure these relationships are independent of a given baseline factor, separating the cohort into this factor's subgroups prior to analysis is necessary. This, however, would reduce power, requiring a larger cohort. It also acknowledged that differing beam conformality and margin recipes across the trials may bias derived associations. For example, the RADAR and CHHiP trials included patients with PTV margins at the prostate posterior reduced to ≤0.5cm and 0cm respectively, potentially increasing the dose at the rectum adjacent to the PTV and the likelihood of a corresponding dose-toxicity association. It must also be noted that patients from the RT01 cohort had the longest follow-up time, while those from CHHiP had the shortest. This means the likelihood of experiencing the considered toxicities would be different for all three trials and this effect was not controlled for. The longest possible follow-up times were considered to maximise power. Finally, it would have been appropriate to exclude patients with acute RB and tenesmus events from the RADAR datasets, to focus on late events. Including these afforded a higher event rate and thus more statistical power, although having only late events in the RADAR datasets would have resulted in these datasets being consistent with datasets from the other two trials. This is recommended for future analyses.

This study has utilised planned dose distributions. These will differ from delivered dose distributions in practice[32]. It has been shown that delivered dose can be a better predictor of rectal toxicity than planned dose[33]. As the consistency between planned and delivered dose improves, or delivered dose

becomes increasingly measurable, voxel-based dose analyses will become more effective in finding anatomically localised dose-outcome relationships. Data derived from patients treated with IGRT, for example, would ensure planned dose more closely resembles delivered dose. Diversity in the dose distributions across the cohort is also limiting, as the mean dose distributions are approximate 3 or 4 field treatments in all datasets (see Appendix Section 4). Greater diversity in technique will enable more generalisable feature selection. The accuracy of registration and the appropriateness of the choice of exemplar and anti-exemplar could also impact derived results. A perfectly accurate registration would ensure associations are in fact occurring at corresponding anatomical sites. To increase computational speed in light of restricted time, 1 in 2 voxels in each dimension were sampled for the T1 and T2 templates. This may have impacted results from the uni-voxel and multivoxel Cox regression tests. It is expected that including less voxels in the tests will most likely may have resulted in less voxels found to show a significant dose-toxicity correlation. This is indicated by the fact that the corresponding (full resolution) T3 results show a larger proportion of significant voxels identified by these tests (see Appendix Section 3). This is a potential source of bias in comparing results across the three templates, and it is therefore recommended that the sampling resolution be made equivalent across all templates in future voxel-based analyses. Finally, deformable image registration (DIR) methods have been used to deform dose distributions onto registration templates. This can lead to dosimetric inaccuracies that could impact derived associations which have not been accounted for[34,35]. Deformations were constrained to that which is physically achievable, preventing tissue from 'folding back in on itself' to help mitigate impact, however it is recommended that future studies seek to conform to appropriate DIR validation protocols as they emerge[36].

This study enabled the identification of unexpected underlying dose-toxicity aetiology with the potential to use this knowledge to develop new treatment approaches or refine existing ones. Incorporating the voxel-based evidence into normal tissue complication probability (NTCP) models may be one such approach, capable of facilitating translation of these results into clinical practice. Palma et al have derived a new NTCP philosophy to include voxel-based evidence of OAR radio-sensitivity[37]. Incorporating the evidence of OAR sensitivity from this study into a model like this could result in reduced toxicity for patients when applied to treatment planning. It is also acknowledged that the majority of evidence discovered in this study was from 3D-CRT patients. Therefore, the methods here may need to be applied to a larger cohort of patients treated with contemporary techniques before translation is made to the clinic.

This was the first study performing a full voxel-based analysis of dose-rectal toxicity relationships indiscriminately throughout the entire pelvic anatomy. Previous studies have established a relationship between high doses in small rectal volumes and resulting bleeding, and subsequent studies have determined predictive rectal subregions[14,15]. This study has reinforced this rectal dose-bleeding relationship, further substantiating the work done in moving toward defining constraints based on subregions as opposed to whole-rectum DVHs. This study has also uniquely identified broader dose-rectal toxicity patterns. Namely that the use of posteriorly extended lateral beams may produce rectal dose hotspots not prevented by conventional dose constraints, resulting in increased incidence of late RB. Also, the use of the posterior beam can lead to higher low-intermediate doses in the PRFS, increasing risk of tenesmus and potentially other control related symptoms.

ACKNOWLEDGEMENTS

We acknowledge funding from the Australian National Health and Medical Research Council (grants 300705, 455521, 1006447, 1077788), the Hunter Medical Research Institute, the Health Research Council (New Zealand), the University of Newcastle, the Calvary Mater Newcastle, the Medical Research Council Clinical Trials Unit at University College London, Abbott Laboratories and Novartis Pharmaceuticals. We acknowledge funding form the Medical Research Council UK (grant MC_UU_12023/28) for the MRC RT01 trial. David Dearnaley, Emma Hall and Sarah Gulliford

acknowledge NHS funding to the National Institute for Health Research (NIHR) Biomedical Research Centre at the Royal Marsden NHS Foundation Trust and The Institute of Cancer Research, London. We acknowledge support of Cancer Research UK (C8262/A7253, C1491/A9895, C1491/A15955, SP2312/021), the Department of Health, the NIHR Cancer Research Network for the CHHiP trial. We acknowledge all trial investigators and patients who've made this study possible. We gratefully acknowledge the support of the Sir Charles Gairdner Hospital, Rachel Kearvell, the 'Elvis' study team including Kristie Harrison, participating RADAR centres, the Trans Tasman Radiation Oncology Group, Ben Hooton and Elizabeth van der Wath. We are also grateful for the contributions of Oscar Acosta, Renaud de Crevoisier, and Eugenia Mylona.

REFERENCES

1. Zelefsky, M. J. *et al.* Incidence of late rectal and urinary toxicities after three-dimensional conformal radiotherapy and intensity-modulated radiotherapy for localized prostate cancer. *Int. J. Radiat. Oncol. Biol. Phys.* **70**, 1124–1129 (2008).

2. Denham, J. W. *et al.* Rectal and urinary dysfunction in the TROG 03.04 RADAR trial for locally advanced prostate cancer. *Radiother. Oncol.* **105**, 184–192 (2012).

3. Wortel, R. C. *et al.* Acute toxicity after image-guided intensity modulated radiation therapy compared to 3D conformal radiation therapy in prostate cancer patients. *Int. J. Radiat. Oncol. Biol. Phys.* **91**, (2015).

4. Cambria, R. *et al.* Evaluation of Late Rectal Toxicity after Conformal Radiotherapy for Prostate Cancer A Comparison between Dose-Volume Constraints and NTCP Use. *Strahlenther Onkol* **185**, 384–390 (2009).

5. Marks, L. B. *et al.* Use of normal tissue complication probability models in the clinic. *Int. J. Radiat. Oncol. Biol. Phys.* **76**, S10–S19 (2010).

6. Landoni, V. *et al.* Predicting toxicity in radiotherapy for prostate cancer. *Phys. Medica* **32**, 521–532 (2016).

7. Thor, M. *et al.* Inter-institutional analysis demonstrates the importance of lower than previously anticipated dose regions to prevent late rectal bleeding following prostate radiotherapy. *Radiother. Oncol.* **127**, 88–95 (2018).

8. Munbodh, R., Jackson, A., Bauer, J., Schmidtlein, C. R. & Zelefsky, M. J. Dosimetric and anatomic indicators of late rectal toxicity after high-dose intensity modulated radiation therapy for prostate cancer. *Med. Phys.* **35**, 2137–2150 (2008).

9. Buettner, F. *et al.* Assessing correlations between the spatial distribution of the dose to the rectal wall and late rectal toxicity after prostate radiotherapy: an analysis of data from the MRC RT01 trial (ISRCTN 47772397). *Phys. Med. Biol.* **54**, 6535–48 (2009).

10. Buettner, F., Gulliford, S. L., Webb, S. & Partridge, M. Modeling late rectal toxicities based on a parameterized representation of the 3D dose distribution. *Phys. Med. Biol.* **56**, 2103–2118 (2011).

11. Moulton, C. R. *et al.* Spatial features of dose – surface maps from deformably-registered plans correlate with late gastrointestinal complications. *Phys. Med. Biol.* **62**, 4118–4139 (2017).

12. Onjukka, E. *et al.* Patterns in ano-rectal dose maps and the risk of late toxicity after prostate IMRT. *Acta Oncol. (Madr).* **58**, 1757–1764 (2019).

13. Heemsbergen, W. D., Incrocci, L., Pos, F. J., Heijmen, B. J. M. & Witte, M. G. Local dose effects for late gastrointestinal toxicity after hypofractionated and conventionally fractionated modern radiotherapy for prostate cancer in the HYPRO trial. *Front. Oncol.* **10**, (2020).

14. Acosta, O. *et al.* Voxel-based population analysis for correlating local dose and rectal toxicity in prostate cancer radiotherapy. *Phys. Med. Biol.* **58**, 2581–2595 (2013).

15. Dréan, G. *et al.* Identification of a rectal subregion highly predictive of rectal bleeding in prostate cancer IMRT. *Radiother. Oncol.* **119**, 388–397 (2016).

16. Chen, C., Witte, M., Heemsbergen, W. & van Herk, M. Multiple comparisons permutation test for image based data mining in radiotherapy. *Radiat. Oncol.* **8**, 293 (2013).

17. Ospina, J. D. *et al.* Spatial nonparametric mixed-effects model with spatial-varying coefficients for analysis of populations. in *International Workshop on Machine Learning in Medical Imaging* 142–150 (Springer, 2011).

18. Kennedy, A. *et al.* Similarity clustering based atlas selection for pelvic CT image segmentation. *Med. Phys.* **46**, 2246–2250 (2019).

19. Bentzen, S. M. *et al.* Bioeffect modeling and equieffective dose concepts in radiation oncology-Terminology, quantities and units. *Radiother. Oncol.* **105**, 266–268 (2012).

20. Pavi, J., Denekamp, J. & Letschert, J. LENT-SOMA scales for all anatomic sites. *Int J Radiat Oncol Biol Phys* **31**, 1049–1091 (1995).

21. VanderWeele, T. J. & Shpitser, I. On the definition of a confounder. *Ann. Stat.* **41**, 196–220 (2013).

22. Marcello, M. *et al.* Association between treatment planning and delivery factors and disease progression in prostate cancer radiotherapy: Results from the TROG 03.04 RADAR trial. *Radiother. Oncol.* **126**, 249–256 (2018).

23. Tibshiranit, B. R. Regression Shrinkage and Selection via the Lasso. *J. R. Stat. Soc. Ser. B* **58**, 267–288 (1996).

24. Yushkevich, P. A. *et al.* User-guided 3D active contour segmentation of anatomical structures: Significantly improved efficiency and reliability. *Neuroimage* **31**, 1116–1128 (2006).

25. Ebert, M. A. *et al.* Gastrointestinal Dose-Histogram Effects in the Context of Dose-Volume Constrained Prostate Radiation Therapy : Analysis of Data From the RADAR Prostate Radiation Therapy Trial. *Int. J. Radiat. Oncol. Biol. Phys.* **91**, 595–603 (2014).

26. Dréan, G. *et al.* Identification of a rectal subregion highly predictive of rectal bleeding in prostate cancer IMRT. *Radiother. Oncol.* **119**, 388–397 (2016).

27. Colaco, R. J. *et al.* Rectal Toxicity After Proton Therapy For Prostate Cancer : An Analysis of Outcomes of Prospective Studies Conducted at the University of Florida Proton Therapy Institute. *Radiat. Oncol. Biol.* **91**, 172–181 (2014).

28. Fukahori, M., Matsufuji, N., Himukai, T., Kanematsu, N. & Mizuno, H. Estimation of late rectal normal tissue complication probability parameters in carbon ion therapy for prostate cancer. *Radiother. Oncol.* **118**, 136–140 (2016).

29. Moulton, C. R. *et al.* Prostate external beam radiotherapy combined with high-dose-rate brachytherapy: dose-volume parameters from deformably-registered plans correlate with late

gastrointestinal complications. *Radiat. Oncol.* 1–13 (2016). doi:10.1186/s13014-016-0719-2

30. Reis, E. D., Vine, A. J. & Heimann, T. Radiation damage to the rectum and anus: Pathophysiology, clinical features and surgical implications. *Color. Dis.* **4**, 2–12 (2002).

31. Gulliford, S. L. *et al.* Radiotherapy dose-distribution to the perirectal fat space (PRS) is related to gastrointestinal control-related complications. *Clin. Transl. Radiat. Oncol.* **7**, 62–70 (2017).

32. Colvill, E. *et al.* Multileaf Collimator Tracking Improves Dose Delivery for Prostate Cancer Radiation Therapy : Results of the First Clinical Trial. *Radiat. Oncol. Biol.* **92**, 1141–1147 (2015).

33. Shelley, L. E. A. *et al.* Delivered dose can be a better predictor of rectal toxicity than planned dose in prostate radiotherapy. *Radiother. Oncol.* **123**, 466–471 (2017).

34. Salguero, F. J., Saleh-Sayah, N. K., Yan, C. & Siebers, J. V. Estimation of three-dimensional intrinsic dosimetric uncertainties resulting from using deformable image registration for dose mapping. *Med. Phys.* **38**, 343–353 (2011).

35. Vickress, J., Battista, J., Barnett, R. & Yartsev, S. Representing the dosimetric impact of deformable image registration errors. *Phys. Med. Biol.* **62**, N391 (2017).

36. Paganelli, C., Meschini, G., Molinelli, S., Riboldi, M. & Baroni, G. Patient-specific validation of deformable image registration in radiation therapy: Overview and caveats. *Med. Phys.* **45**, e908–e922 (2018).

37. Palma, G., Monti, S., Buonanno, A., Pacelli, R. & Cella, L. PACE: a probabilistic atlas for normal tissue complication estimation in radiation oncology. *Front. Oncol.* **9**, (2019).

FIGURE CAPTIONS

Figure 1 *Visual representation of the a) Voxel-Based Dose Difference Permutation Test, b) Uni-Voxel Cox Regression test and c) Multi-Voxel Cox Regression Test with LASSO Feature Selection.*

Figure 2 *Results for rectal bleeding. Corresponding axial, coronal and sagittal slices (top to bottom) of a) mean dose difference maps and significant dose difference regions determined by permutation test, b) uni-voxel Cox regression HR and p-value maps and c) multi-voxel Cox regression LASSO HR maps (with uni-voxel p-values for comparison), for respective data sets. 'No Voxels Selected' implies the LASSO selected no voxels of significant correlation with the endpoint within the patient region. The slices chosen for display are those which coincide with the most dominant emergent dose-endpoint patterns, indicated in corresponding planes with dashed lines. Tones of red correspond to regions where increased dose is associated with incidence of dysuria (HR > 1), while tones of blues correspond to regions where reduced dose is associated with incidence of dysuria (HR < 1). The CTV is delineated in orange while the bladder and rectum are delineated in yellow. Anatomical directions left (L), right (R), superior (S), inferior (I), anterior (A), and posterior (P) are also indicated.*

Figure 3 *Results for tenesmus. Corresponding axial, coronal and sagittal slices (top to bottom) of a) mean dose difference maps and significant dose difference regions determined by permutation test, b) uni-voxel Cox regression HR and p-value maps and c) multi-voxel Cox regression LASSO HR maps (with uni-voxel p-values for comparison), for respective data sets. 'No Voxels Selected' implies the LASSO selected no voxels of significant correlation with the endpoint within the patient region. The slices chosen for display are those which coincide with the most dominant emergent dose-endpoint patterns, indicated in corresponding planes with dashed lines. Tones of red correspond to regions where increased dose is associated with incidence of dysuria (HR > 1), while tones of blues correspond to regions where reduced dose is associated with incidence of dysuria (HR < 1). The CTV is delineated in orange while the bladder and rectum are delineated in yellow. Anatomical directions left (L), right (R), superior (S), inferior (I), anterior (A), and posterior (P) are also indicated.*

Figure 4 *a) The mean planned dose distribution for the combined cohort. Displayed on the map are the significant dose difference regions determined by the permutation test for both RB ($p<0.3$) and tenesmus ($p<0.05$), with the mean doses and dose differences at a representative voxel within those regions highlighted for each outcome. b) The standard deviation planned dose distribution for the combined cohort. Similarly displayed are the permutation test result regions, with the standard deviation dose at a voxel at the centre of the rectal bleeding region.*

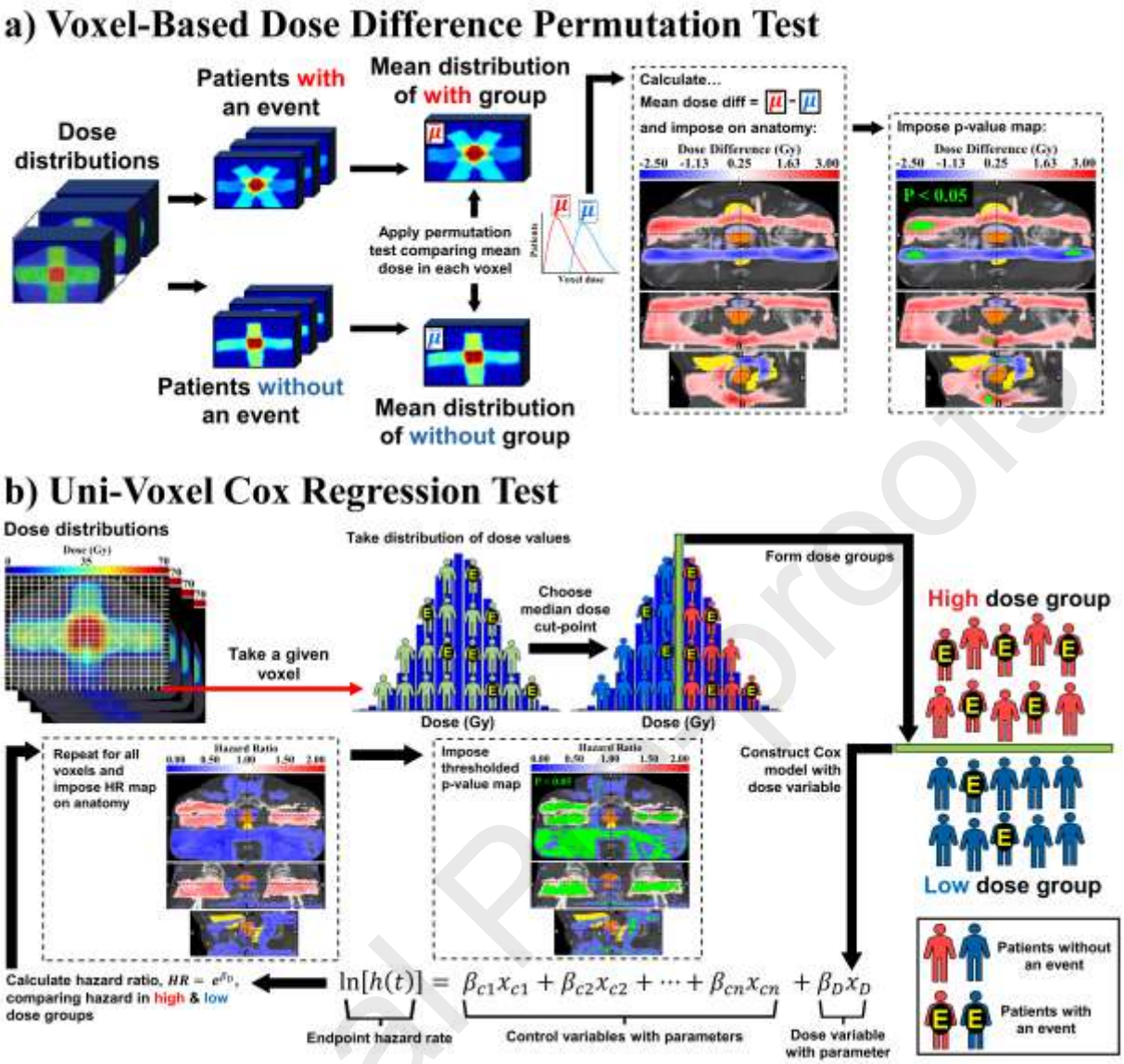

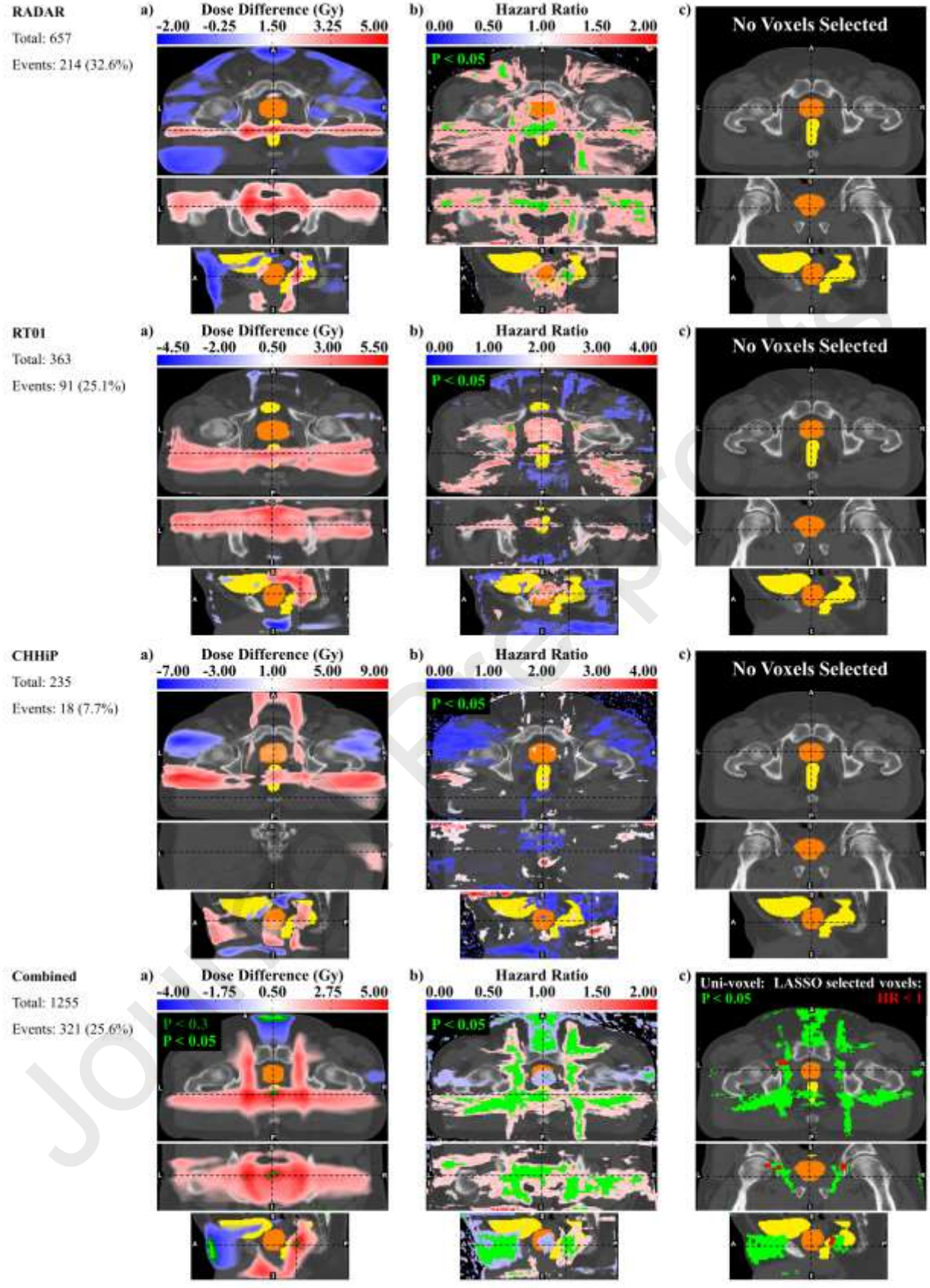
RADAR
Total: 657
Events: 214 (32.6%)
a) Dose Difference (Gy)
-2.00 -0.25 1.50 3.25 5.00
b) Hazard Ratio
0.00 0.50 1.00 1.50 2.00
P < 0.05
c) No Voxels Selected
RT01
Total: 363
Events: 91 (25.1%)
a) Dose Difference (Gy)
-4.50 -2.00 0.50 3.00 5.50
b) Hazard Ratio
0.00 1.00 2.00 3.00 4.00
P < 0.05
c) No Voxels Selected
CHHiP
Total: 235
Events: 18 (7.7%)
a) Dose Difference (Gy)
-7.00 -3.00 1.00 5.00 9.00
b) Hazard Ratio
0.00 1.00 2.00 3.00 4.00
P < 0.05
c) No Voxels Selected
Combined
Total: 1255
Events: 321 (25.6%)
a) Dose Difference (Gy)
-4.00 -1.75 0.50 2.75 5.00
P < 0.3
P < 0.05
b) Hazard Ratio
0.00 0.50 1.00 1.50 2.00
P < 0.05
c) Uni-voxel: LASSO selected voxels:
P < 0.05
HR < 1

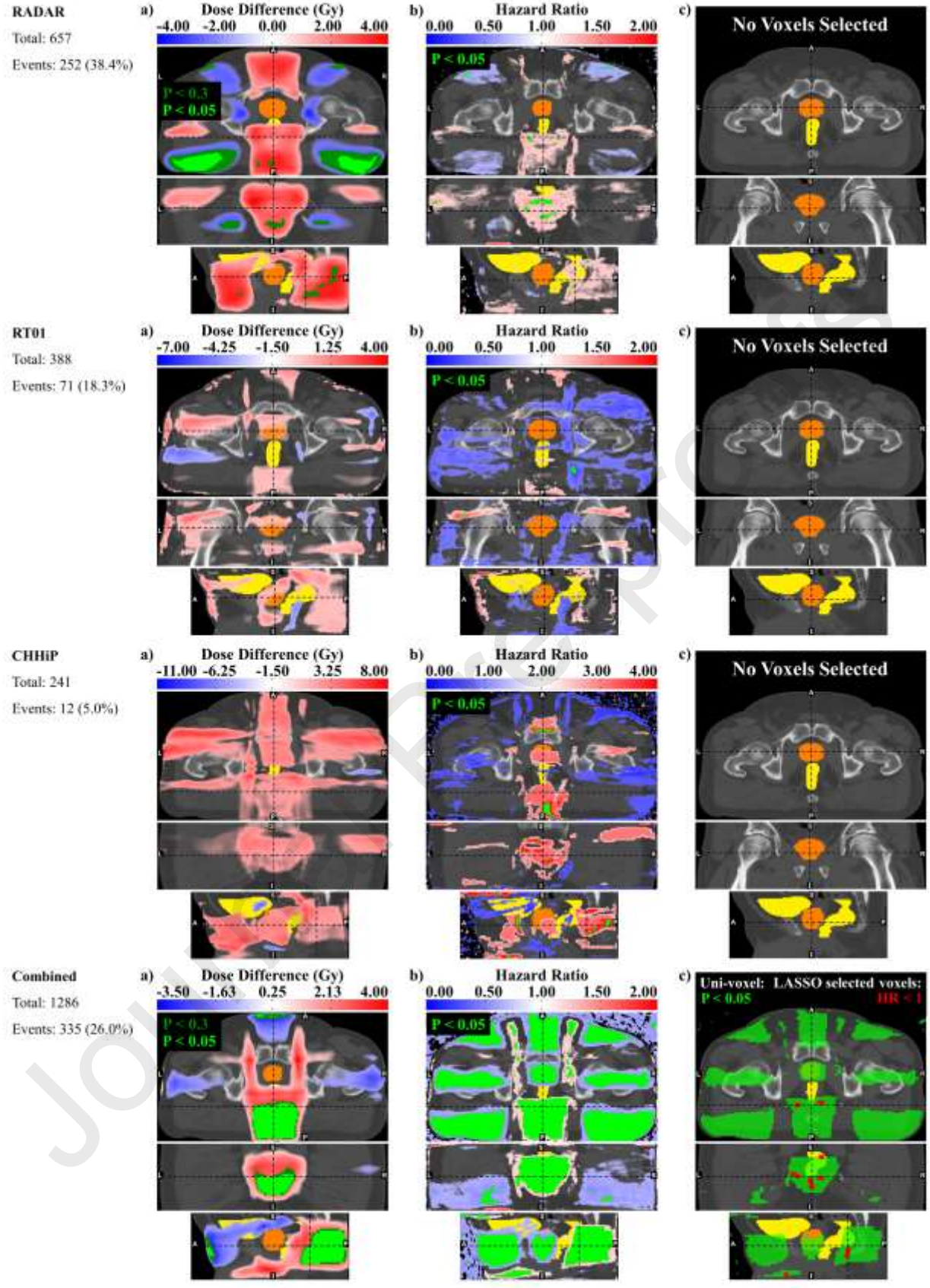
RADAR
Total: 657
Events: 252 (38.4%)
a) Dose Difference (Gy)
-4.00 -2.00 0.00 2.00 4.00
P < 0.3
P < 0.05
b) Hazard Ratio
0.00 0.50 1.00 1.50 2.00
P < 0.05
c) No Voxels Selected
RT01
Total: 388
Events: 71 (18.3%)
a) Dose Difference (Gy)
-7.00 -4.25 -1.50 1.25 4.00
b) Hazard Ratio
0.00 0.50 1.00 1.50 2.00
P < 0.05
c) No Voxels Selected
CHHiP
Total: 241
Events: 12 (5.0%)
a) Dose Difference (Gy)
-11.00 -6.25 -1.50 3.25 8.00
b) Hazard Ratio
0.00 1.00 2.00 3.00 4.00
P < 0.05
c) No Voxels Selected
Combined
Total: 1286
Events: 335 (26.0%)
a) Dose Difference (Gy)
-3.50 -1.63 0.25 2.13 4.00
P < 0.3
P < 0.05
b) Hazard Ratio
0.00 0.50 1.00 1.50 2.00
P < 0.05
c) Uni-voxel: LASSO selected voxels:
P < 0.05
HR < 1

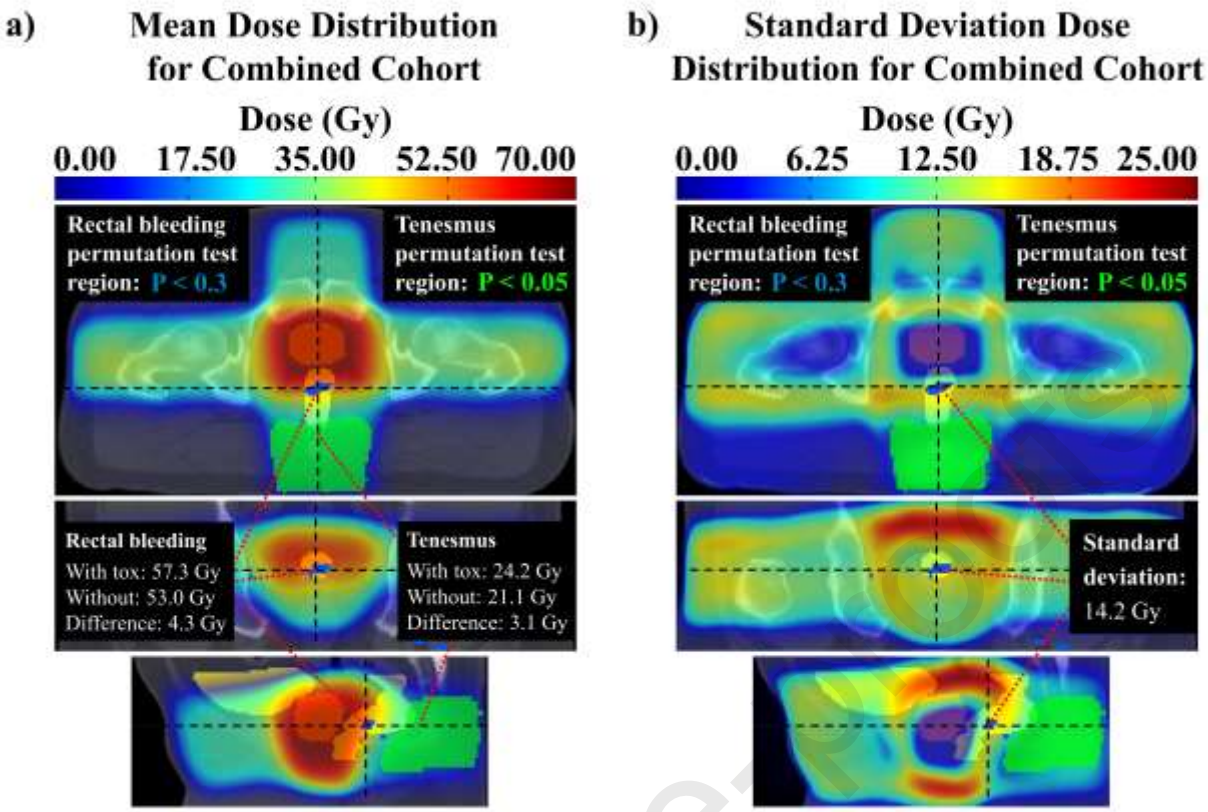

Table 1 *Clinical trials information.*

	RADAR	RT01	CHHiP
Full name	Randomised Androgen Deprivation and Radiotherapy (TROG 03.04) Trial[20,21]	A Randomised Trial of High Dose Therapy in Localised Cancer of the Prostate using Conformal Radiotherapy Techniques[22,23]	Conventional or Hypofractionated High Dose Intensity Modulated Radiotherapy for Prostate Cancer Trial[24,25]
Descriptors	• Randomised • Phase 3 • Factorial	• Randomised • Phase 3 • Superiority	• Randomised • Phase 3 • Non-inferiority
Goal	Comparison of 6 months of androgen deprivation therapy (ADT) plus radiotherapy with 18 months of ADT with the same radiotherapy	Comparison of 64 Gy standard-dose and 74 Gy dose-escalated conformal radiotherapy	Comparison of conventional and hypofractionated IMRT
Countries	Australia and New Zealand	United Kingdom, New Zealand, Australia	United Kingdom, New Zealand, Rep. of Ireland, Switzerland
Accrual years	Oct 2003 – Aug 2007	Jan 1998 – Dec 2001	Oct 2002 – Jun 2011
Total accrued subjects	1071	843	3216
Date data was frozen	June 2015	Aug 2013	Oct 2017
Participants	Intermediate-risk (T2a) or high-risk (T2b+) prostate cancer	T1b – T3a prostate cancer	T1b – T3a prostate cancer
Radiotherapy type	Dose escalated 3D conformal EBRT	Standard or dose escalated 3D conformal EBRT	Dose escalated IMRT
Prescribed dose groups (dose per fraction)	66 Gy (2 Gy), 70 Gy (2 Gy), 74 Gy (2 Gy)	64 Gy (2 Gy), 74 Gy (2 Gy)	57 Gy (3 Gy), 60 Gy (3 Gy), 74 Gy (2 Gy)
Rectal dose-volume constraints	Maximum of 65 Gy, 70 Gy and 75 Gy to 40%, 30% and 5% of rectal volume respectively	A maximum of 64 Gy and 74 Gy to any volume of the rectum for each dose group respectively	Maximum of 65 Gy, 70 Gy and 75 Gy to 30%, 15% and 3% of rectal volume respectively
Beam arrangements	Any preferred combination of 3 or more conformal beams	3 or 4 beams (anterior/lateral/posterior) for first 64 Gy, with additional 4 or 6 beam boost to 74 Gy	3 or 4 beams (anterior/lateral/posterior) or 5 beams or more if inverse planning utilised
Electronic review of treatment planning data	Full retrospectve review for all subjects[26]	No electronic individual plan review[27]	Full prospective case reviews for the first 2 or 3 subjects at each centre[28]
Manager	TROG Cancer Research, NSW, Australia	Medical Research Clinical Trials Unit, London, UK	Clinical Trials and Statistics Unit, the Institute of Cancer Research, London, UK
Trial registration number	ISRCTN90298520	ISRCTN47772397	ISRCTN97182923
Ethics approval number	Approved by Hunter New England Human Research Ethics Committee Trial ID 03/06/11/3.02	North Thames Multi-centre Research Ethics Committee number MREC/97/2/16	Approved by the London Multi-centre Research Ethics Committee number 04/MRE02/10

RADAR				RT01			CHHiP			COMBINED		
		Bleeding (grade≥2)	**Tenesmus (grade≥2)**		**Bleeding (grade≥2)**	**Tenesmus (grade≥2)**		**Bleeding (grade≥2)**	**Tenesmus (grade≥2)**		**Bleeding (grade≥2)**	**Tenesmus (grade≥2)**
Total number of subjects		657	657	**Total number of subjects**	363	388	**Total number of subjects**	235	241	**Total number of subjects**	1225	1286
Events		214 (32.6%)	252 (38.4%)	**Events**	91 (25.1%)	71 (18.3%)	**Events**	18 (7.7%)	12 (5.0%)	**Events**	321 (25.6%)	335 (26.0%)
Follow-up in months (min, max, med, IQR)		(3, 96, 48, 54)	(3, 96, 42, 60)	**Follow-up in months (min, max, med, IQR)**	(6, 147, 72, 62)	(12, 158, 98, 65)	**Follow-up in months (min, max, med, IQR)**	(6, 68, 60, 2)	(6, 68, 60, 2)	**Follow-up in months (min, max, med, IQR)**	(3, 147, 60, 36)	(3, 158, 6 59)
Variables	**Definitions**			**Definitions**			**Definitions**			**Definitions**		
Age[1]	**Median**	69.4 yrs	69.4 yrs	**Median**	68.0 yrs	67.9 yrs	**Median**	67.3 yrs	67.4 yrs	**Median**	68.5 yrs	68.5 yrs
Prescribed dose	**[66 Gy]**	82	82	**[64 Gy]**	173	204	**[57 Gy]**	72	86	**[66 Gy (RADAR), 64 Gy (RT01), 57 Gy and 60 Gy (CHHiP)]**	373	453
	[70 Gy]	366	366	**[74 Gy]**	190	184	**[60 Gy]**	70	80			
	[74 Gy]	209	209				**[74 Gy]**	64	75		882	833
										[70 Gy and 74 Gy (RADAR), 74 Gy (RT01), 74 Gy (CHHiP)]		
Disease risk	**[GS ≤ 7]**	461	461	**[T1b/c or T2a with (PSA + (GS - 6)*10) < 15]**	98	110	**[T1b/c or T2a with PSA ≤ 10 and GS ≤ 6]**	51	58	**[Lower risk group subjects from each respective dataset]**	617	883
	[GS > 7]	196	196		265	278		155	183		638	403
				[T1b/c or T2a with (PSA + (GS - 6)*10) ≥ 15 or T2b/T3a]			**[Any of the following: Stage ≥ T2b, 10 < PSA ≤ 20, GS > 6]**			**[Higher risk group subjects from each respective dataset]**		
Cancer stage	**[T2]**	473	473	**[≤ T2a (T1b, T1c, T2a)]**	221	235	**[≤ T2a (T1a, T1b, T1c, T2a)]**	174	175	**[Lower cancer stage group subjects from each respective dataset]**	865	885
	[T3/T4]	184	184		142	153		61	66		390	406
				[> T2a (T2b, T3a)]			**[> T2a (T2b, T2c, T3a)]**			**[Higher cancer stage group subjects from each respective dataset]**		
Baseline PSA[1]	**Median**	14.00 ng/ml	14.04 ng/ml	**Median**	13.80 ng/ml	13.80 ng/ml	**Median**	11.70 ng/ml	11.70 ng/ml	**Median**	13.60 ng/ml	13.50 ng/ml
Number of beams	**[3 beams]**	67	67	**[3 beams for phase 1 of treament]**	214	228	**[≤ 4 beams]**	204	210	**[≤ 4 beams (RADAR), 3 beams (RT01), ≤ 4 beams (CHHiP)]**	840	858
	[4 beams]	350	350		149	160	**[> 4 beams]**	31	31		415	428
	[5 beams]	88	88									
	[6 beams]	93	93	**[4 beams for phase 1 of treament]**						**[> 4 beams (RADAR),**		

beams]

4 beams (RT01), > 4 beams (CHHiP)]

***Table 2** The number of subjects in each trial dataset, broken down by endpoint and patient control variables, in*

[1]This variable was divided into two approximately equal subgroups split about the median value

Highlights

- Voxel-wise analysis correlated rectal toxicities with dose in the pelvic anatomy.
- Grade ≥ 2 bleeding correlated with high doses to a small rectal volume.
- This confirmed the serial response of the rectum with respect to rectal bleeding.
- Grade ≥ 2 tenesmus correlated with low-intermediate doses to the perirectal fat space.
- This demonstrated the parallel response of the PRFS with respect to tenesmus.

CONFLICTS OF INTEREST

Professor Dearnaley discloses that his employer, the Institute of Cancer Research, receives royalty income from abiraterone. I receive a share of this income through the ICR's Rewards to Discoverers Scheme.

Mr Sydes reports grants from Health Data Research UK, during the conduct of the study; personal fees from Lilly Oncology, personal fees from Janssen, grants and non-financial support from Astellas, grants and non-financial support from Clovis Oncology, grants and non-financial support from Janssen, grants and non-financial support from Novartis, grants and non-financial support from Pfizer, grants and non-financial support from Sanofi-Aventis, outside the submitted work.

Professor Hall reports grants from Cancer Research UK, during the conduct of the study; grants from Accuray Inc., outside the submitted work.

Professor Ebert reports grants from Australian National Health and Medical Research Council, during the conduct of the study.

All other authors declared no conflicts of interest.